Electronic Supplementary Material

Continuous amino-functionalized University of Oslo 66 membranes as efficacious polysulfide barriers for lithium-sulfur batteries

Bowen Du, Yuhong Luo, Feichao Wu (✉), Guihua Liu, Jingde Li (✉), Wei Xue (✉)

Hebei Provincial Key Laboratory of Green Chemical Technology and High Efficient Energy Saving, School of Chemical Engineering and Technology, Hebei University of Technology, Tianjin 300130, China

E-mails: wufeichao321@hebut.edu.cn (Wu F); jingdeli@hebut.edu.cn (Li J); weixue@hebut.edu.cn (Xue W)

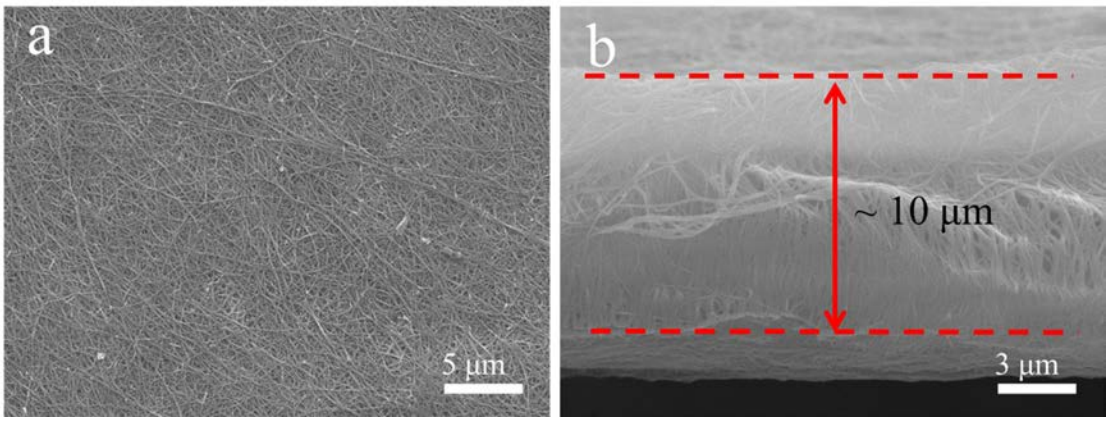

Fig. S1. (a) Surface and (b) cross-section SEM image of the CNT film.

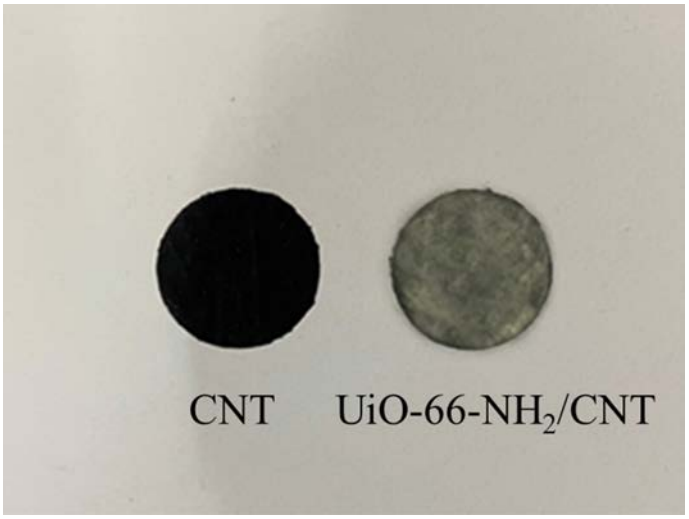

Fig. S2. Digital photos of CNT film and UiO-66-NH_2/CNT.

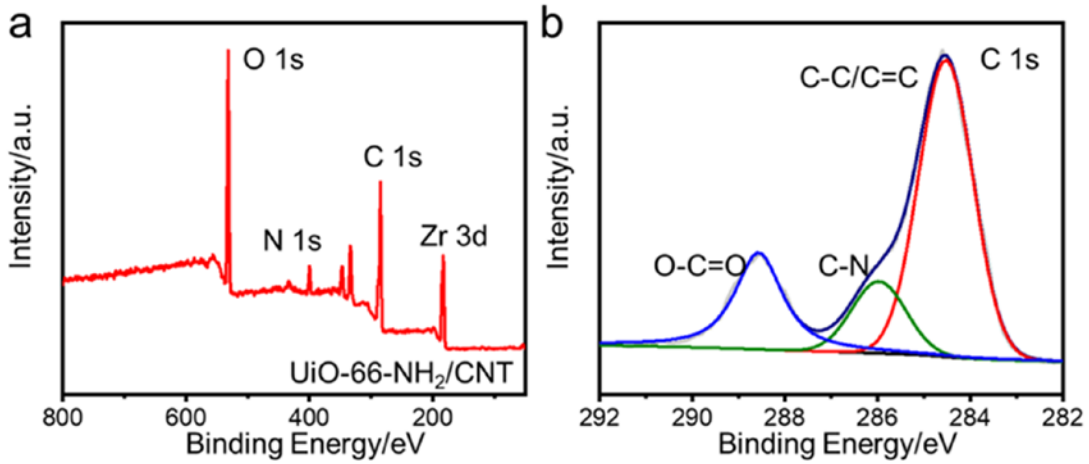

Fig. S3. (a) XPS survey and (b) C 1s spectra of UiO-66-NH_2/CNT.

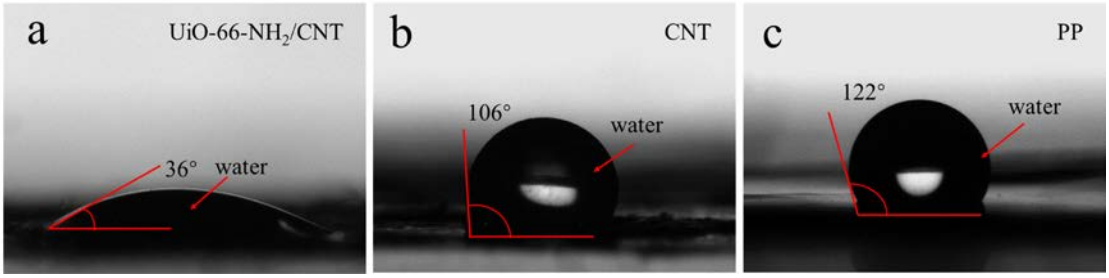

Fig. S4. Water contact angles over the surface of (a) UiO-66-NH_2/CNT, (b) CNT film and (c) PP separator.

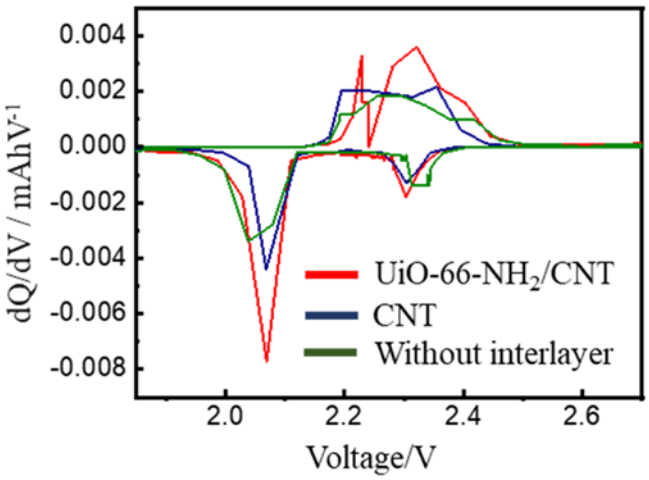

Fig. S5. The dQ/dV plots of the 5th cycle for different interlayers.

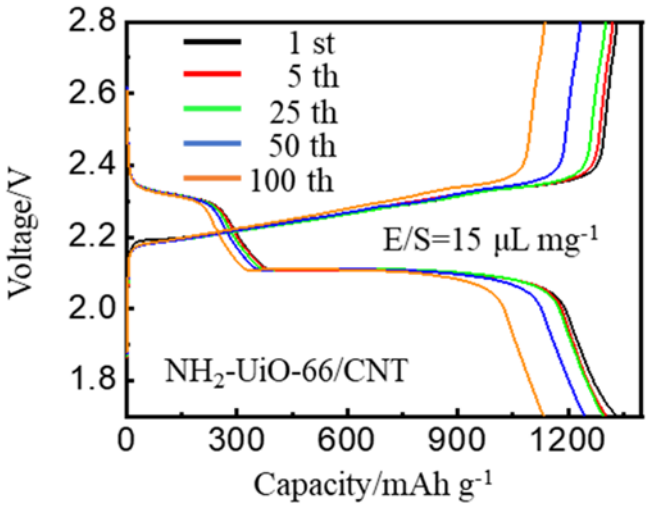

Fig. S6. Galvanostatic discharge-charge profiles for the UiO-66-NH_2/CNT interlayer at 0.2 C.

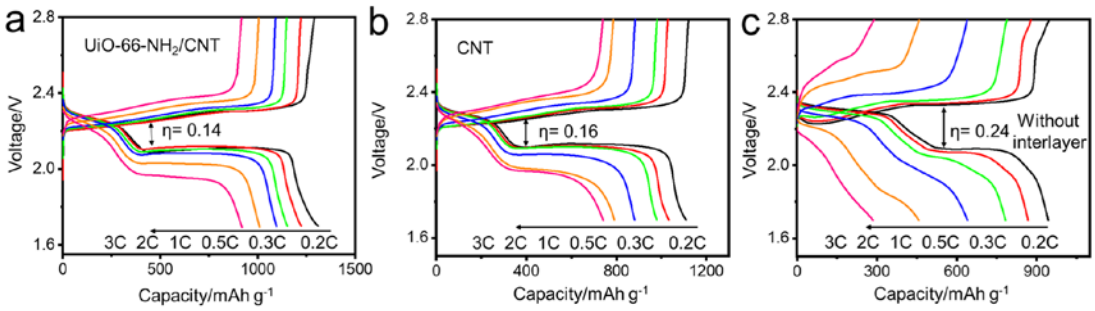

Fig. S7. Constant discharge/charge curves for batteries with different interlayers under diverse current densities.

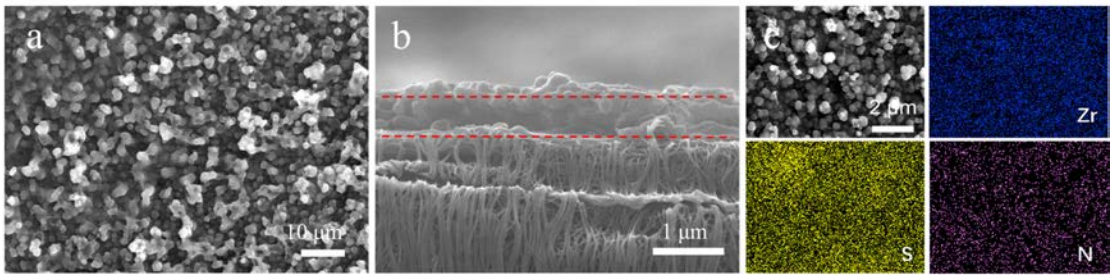

Fig. S8. (a) surface, (b) cross-section SEM image and (c) elemental mapping of the UiO-66-NH_2/CNT after cycled at 1 C.

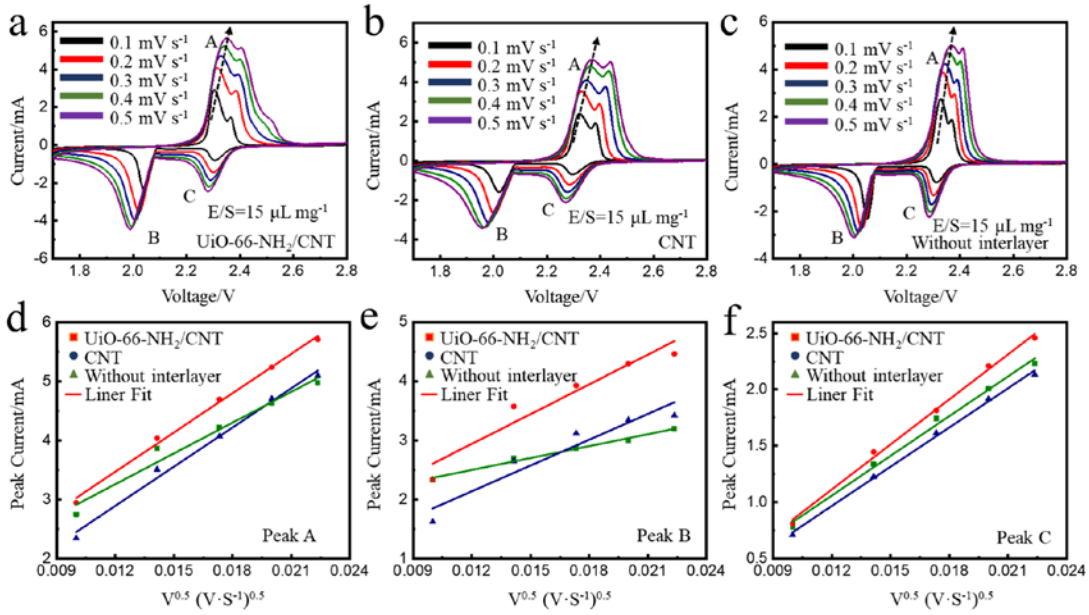

Fig. S9. (a−c) CV curves and (d−f) the relation between the square root of scan rates and peak currents for various interlayers.

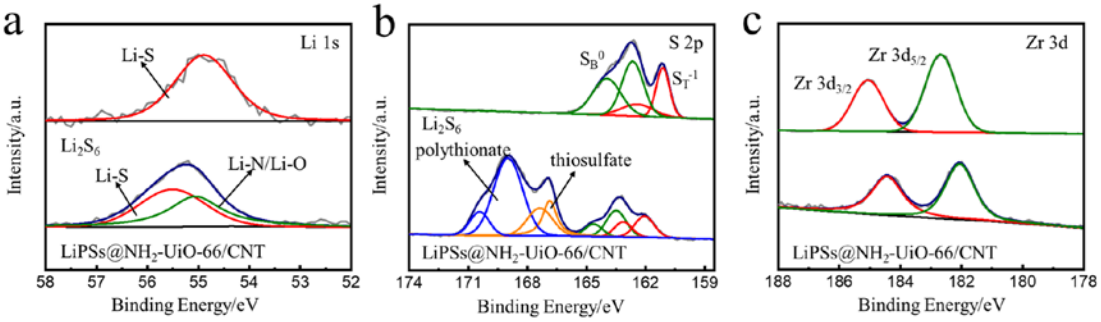

Fig. S10. XPS spectra for L_2S_6 and UiO-66-NH_2/CNT after cycled at 1 C.

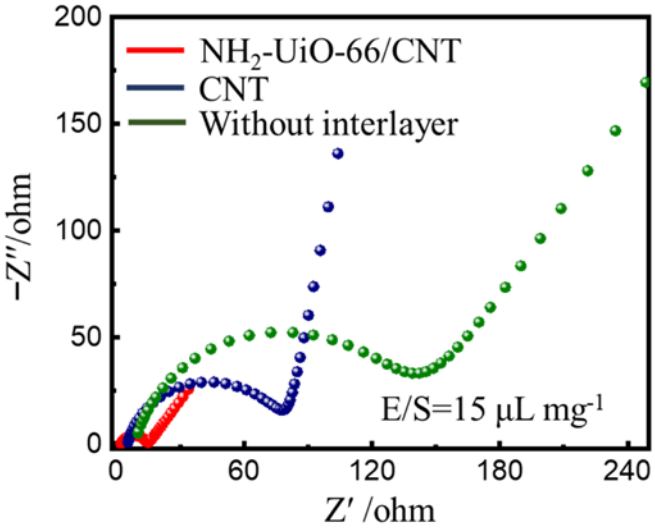

Fig. S11. EIS for the cells after 100 cycles at 0.2 C.

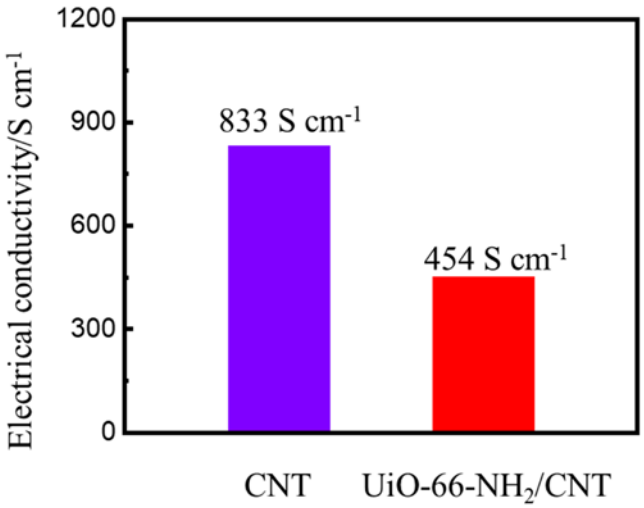

Fig. S12. Electrical conductivity of CNT film and UiO-66-NH_2/CNT.

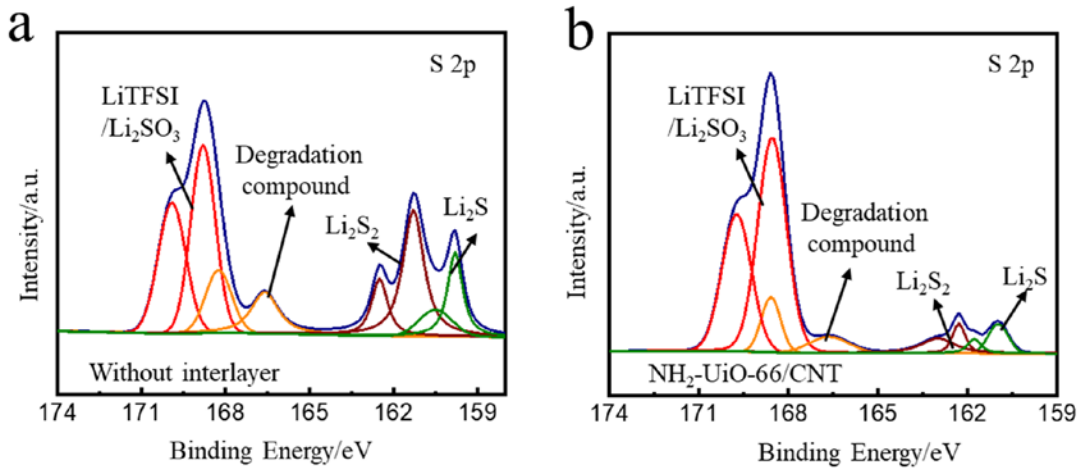

Fig. S13. XPS analysis on the Li anodes from cells with (a) no interlayer and (b) UiO-66-NH_2/CNT interlayer after cycling at 1 C.

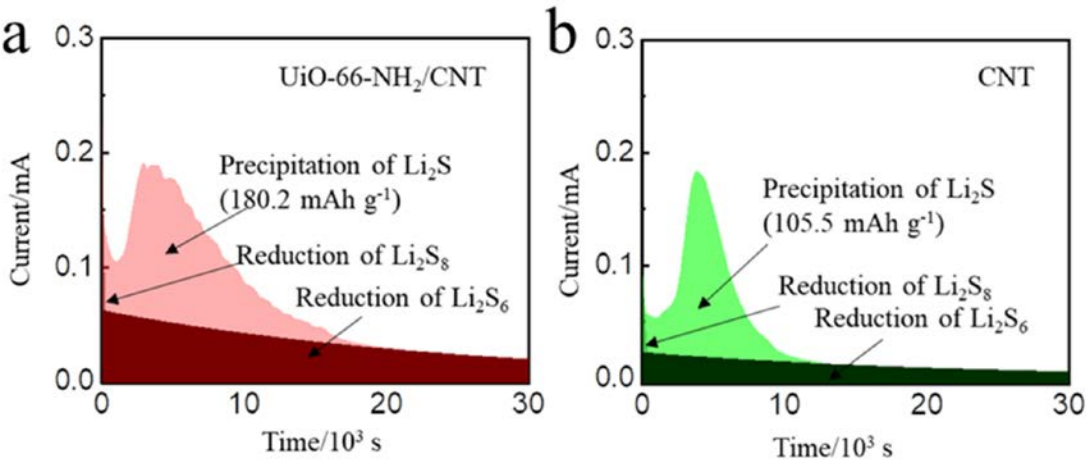

Fig. S14. Li_2S precipitation test of UiO-66-NH_2/CNT and CNT film.

Table S1. The electrochemical performance of different interlayers in recent literatures.

Structures	S load (mg cm^{-2})	Interlayer mass load (mg cm^{-2})	capacity (mAh g^{-1}) /C rate	Rate (mAh g^{-1}) /C rate	Capacity decay /cycle number/C rate	Ref.
UiO-66-NH_2/CNT	**2.1**	**1.34**	**1333.14 (0.2C)**	**919.01 (3C)**	**0.04%/300/1C**	**This work**
UiO−66/PP	1.5	0.35	1032 (0.5C)	461 (2C)	0.03%/500/0.5C	[1]
UiO-66-S/Nafion/PP	1.7	1.0	1185 (0.2C)	785 (3C)	0.11%/200/0.2C	[2]
PPZ-HG-CCP	1.5	3.0	1191.3 (0.2C)	782.4 (3C)	0.015%/500/2C	[3]
CNFO@CNT	1.0–1.2	1.25	1332 (0.1C)	902 (2C)	0.063%/250/2C	[4]
MnO/mCNF	1.5	2.5-3.2	1032 (0.2C)	519 (5C)	0.02%/400/1C	[5]
Cu_2(CuTCPP)	2.0	0.1	1020 (0.2C)	437 (5C)	0.032%/900/1C	[6]
CoS/Co_9S_8@CCNSs	1.3–1.5	2.0-2.3	1392 (0.2C)	600 (1C)	0.018%/500/1C	[7]
Co_9S_8@MoS_2/CNF	3	-	1106 (0.1C)	477 (5C)	0.091%/100/1C	[8]
ZnO-rGO	1.2	-	1664 (0.2C)	810 (2C)	0.04%/500/1C	[9]
Co-MOF-74@MWCNT	1.0	2.9	1434 (0.1C)	802 (2C)	0.23%/175/1C	[10]
MoS_2/CNT	1.4	0.25	1205 (0.2C)	784 (10C)	0.061%/500/0.5C	[11]
CNT/MoP_2	1.2	-	1223 (0.2C)	360 (5C)	0.025%/500/0.1C	[12]

References

1. Fan Y, Niu Z, Zhang F, Zhang R, Zhao Y, Lu G. Suppressing the shuttle effect in lithium-sulfur batteries by a UiO-66-modified polypropylene separator. ACS Omega, 2019, 4(6): 10328–10335

2. Kim S H, Yeon J S, Kim R, Choi K M, Park H S. A functional separator coated with sulfonated metal-organic framework/nafion hybrids for Li-S batteries. Journal of Materials Chemistry A, 2018, 6(48): 24971–24978

3. Chen P, Wu Z, Guo T, Zhou Y, Liu M, Xia X, Sun J, Lu L, Ouyang X, Wang X, et al. Strong chemical interaction between lithium polysulfides and flame-retardant polyphosphazene for lithium-sulfur batteries with enhanced safety and electrochemical performance. Advanced Materials, 2021, 33(9): 1–11

4. Liu T, Sun S, Hao J, Song W, Niu Q, Sun X, Wu Y, Song D, Wu J. Reliable interlayer based on hybrid nanocomposites and carbon nanotubes for lithium-sulfur batteries. ACS Applied Materials and Interfaces, 2019, 11(17): 15607–15615

5. Chen M, Li T, Li Y, Liang X, Sun W, Chen Q. Rational design of a MnO nanoparticle-embedded carbon nanofiber interlayer for advanced lithium-sulfur batteries. ACS Applied Energy Materials, 2020, 3(11): 10793–10801

6. Tian M, Pei F, Yao M, Fu Z, Lin L, Wu G, Xu G, Kitagawa H, Fang X. Ultrathin MOF nanosheet assembled highly oriented microporous membrane as an interlayer for lithium-sulfur batteries. Energy Storage Mater, 2019, 21: 14–21

7. Seo S D, Choi C, Park D, Lee D Y, Park S, Kim D W. Metal-organic-framework-derived 3D crumpled carbon nanosheets with self-assembled Co_xS_y nano catalysts as an interlayer for lithium-sulfur batteries. Chemical Engineering Journal, 2020, 400: 125959

8. Li B, Su Q, Yu L, Zhang J, Du G, Wang D, Han D, Zhang M, Ding S, Xu B. Tuning the band structure of MoS_2 via Co_9S_8@MoS_2 core-shell structure to boost catalytic activity for lithium-sulfur batteries. ACS Nano, 2020, 14(12): 17285–17294

9. Lo Y H, Kuo P L, Wu J J. Direct coating of multifunctional zinc oxide-reduced graphene oxide interlayer on cathode for lithium-sulfur batteries. Electrochimica Acta, 2021, 382: 138270

10. Sung S. H, Kim B H, Lee S T, Choi S, Yoon W. Y. Increasing sulfur utilization in lithium-sulfur batteries by a Co-MOF-74@MWCNT interlayer. Journal of Energy Chemistry, 2021, 60: 186–193

11. Yan L, Luo N, Kong W, Luo S, Wu H, Jiang K, Li Q, Fan S, Duan W, Wang J. Enhanced performance of lithium-sulfur batteries with an ultrathin and lightweight MoS_2/Carbon nanotube interlayer. Journal of Power Sources, 2018, 389: 169–177

12. Luo Y, Luo N, Kong W, Wu H, Wang K, Fan S, Duan W, Wang J. Multifunctional interlayer based on molybdenum diphosphide catalyst and carbon nanotube film for lithium-sulfur batteries. Small, 2018, 14(8): 1–9